Modeling approach of flowing condensate coverage rate on inclined wall for aerosol wash down

Fangnian Wang*, Xu Cheng

Institute for Applied Thermofluidics (IATF), Karlsruhe Institute of Technology (KIT), Germany

ARTICLE INFO

Keywords:
Modeling approach
Flowing condensate
Coverage rate
Droplet
Rivulet
Aerosol wash down

ABSTRACT

The flowing condensate coverage on inclined wall is a significant factor for evaluating the aerosol wash down process in the containment. In this paper a modeling approach of condensate coverage rate is proposed. This approach contains a microscopic treatment (including droplet model, transition criterion and rivulet model) and a macroscopic treatment. The derived parameters, e.g. coverage rate, are in terms of volume flow rate, contact angles, inclination and fluid properties, and can be easily implemented into the containment analysis programs. This approach is validated by several existing experimental data. The comparison results show generally good agreement of the modeling approach with experimental data. Furthermore, the numerical results of a basic case are presented and discussed.

1. Introduction

During severe accident in LWR fission products are released into the containment together with large amount of steam and non-condensable gases. The steam condenses on the cold structures and the condensate flows down the walls and finally reserves in the sump at the containment bottom. Together with the condensing steam gaseous aerosols are transferred into the wall condensate and washed down by the condensate (Weber et al., 2015).

The wash down process governs the distribution of the fission products between structures and water pools. Fission products in the water phase produces steam due to the decay heat as well as decay heat released in dry structures causes a dry heating of the containment. Furthermore, distribution and relocation of radionuclides is important to assess radiation damages of local components like electronic devices, seals, etc. The wash down processes interact with thermal hydraulic and aerosol particle transportation processes in the containment (Weber et al., 2015).

In the containment code COCOSYS, the thermal hydraulics of the aerosol wash down processes is currently modelled in a simplified way (Klein-Heßling et al., 2015). For instance, the aerosol wash down model for insoluble aerosols AULA (German: "**A**bwaschen **un**löslicher **A**erosole") simulates the erosion of insoluble aerosols by flowing condensate. The erosion takes place when the flow shear velocity at the wall exceeds the critical threshold (Shields criterion from sediment transport theory (Guo, 2002)). However, the thermal hydraulics, such as the flow patterns and the condensate coverage rate are considered very empirically. In AULA model, the condensate flow pattern is often considered as rivulets with a specific width and a user given coverage rate. Actually the flow patterns and the coverage rate are dependent on the volume flow rate, contact angles, inclination and fluid properties.

The overall objective of this paper is to develop a modeling approach for describing the flowing condensate behavior and the coverage rate on the inclined wall. Different patterns of condensate flow and the transition from droplet to rivulet are considered. This modeling approach is validated by several sets of experimental data.

2. Modeling approach

The flow patterns under condensation condition have three phases, i.e., the moving droplet, rivulets and fully covered film, as shown in Fig. 1. At beginning the droplet generates on the cooling surface due to the condensation and grows up until its volume reaches the threshold, beyond which the droplet starts to move downward the wall surface. Droplet grows up during its movement, until the transition criterion is satisfied. After transition, rivulet forms and its width spreads with the condensate increases. The last phase is about the film fully covered the structure. The modeling approach should integrate all the understandings of these 3 flow patterns.

Our target is to find a modeling approach, which can figure out the average coverage rate of condensate flow, which should be feasible to use in nuclear containment code. However, the containment code

* Corresponding author.
E-mail address: fangnian.wang@kit.edu (F. Wang).

Nomenclature

A	droplet/rivulet wetting area, m^2
a	initial rivulet half width
Bo	Bond number
Bo_c	critical Bond number where droplet start moving
Bo_t	Bond number where transition happens
d_h	hydraulic diameter of the interface between droplet part 1 and 2, m
d_t	critical droplet diameter where transition happens, m
F_g	gravitation force, N
$F_{i,21}/F_{i,12}$	action and reaction forces on interface, N
F_M	equivalent Marrangoni force, N
F_σ	surface tension force, N
F_τ	viscous forces, N
g	gravity acceleration, m/s^2
h_t	critical height where transition happens, m
Δh_{fg}	specific latent heat of vapor condensation, J/kg
n	droplets initiation density, $1/(m^2 \cdot s)$
q	condensation heat flux, W/m^2
Re	Reynolds number
r	radius of droplet, m
r_t	radius of droplet where transition happens, m
T	temperature, ˚C
u	droplet/rivulet velocity, m/s
V	droplet/rivulet volume, m^3
V_0	droplet onset of motion volume, m^3
ΔV_{cond}	all condensation during movement, m^3
V_t	critical volume where transition happens, m^3
$\dot{V}$	volume flow rate per width, $m^3/(m \cdot s)$
We	Weber number
x	perpendicular direction to the wall
y	normal direction to the wall
Δy	droplet height in y- direction
z	droplet/rivulet moving direction

Greek symbols

α	inclination angle, ˚
δ	droplet/rivulet thickness, m
ε	coverage rate, wetting area ratio
$\theta_{s,A}/\theta_{s,R}$	static advancing and receding contact angle, ˚
$\theta_{d,A}/\theta_{d,R}$	dynamic advancing and receding contact angle, ˚
θ_e	equilibrium contact angle, ˚
μ	water viscosity, Pa·s
ρ	water density, kg/m^3
σ_{LG}	surface tension between water and air, N/m
ϕ	thickness in the two side arc parts

usually can't offer a single droplet or rivulet motion trajectory along wall surface but the total condensate volume flow rate of them. Therefore, the current modeling approach is separated into two steps: microscopic and macroscopic treatment. We consider all the flow patterns in one single droplet or rivulet moving trace in the microscopic treatment, while calculate the amount of droplets or rivulets in the macroscopic treatment. The average thickness and velocity of condensate are expressed as a function of condensate volume flow rate per width, which can be given by containment code. Finally, we get our target: the coverage rate, which is in terms of the volume flow rate per width, and other input parameters.

2.1. Microscopic treatment

This step considers the movement of droplet and rivulet as an isolated single trace – we call it microscopic treatment. The aim of this step is to calculate the condensate volume of moving droplet or rivulet, meanwhile the wetting area, thickness, and velocity are obtained simultaneously. The condensate volume can be expressed as the Eq. (1). V_0 is the droplet volume at its onset of motion, beyond which the droplet starts to move downwards. ΔV_{cond} is the volume increase of the moving droplet due to condensation during its movement, which is the integral of all condensate along the moving trace, see Fig. 2. Since both wetting area$A$ and velocity u of droplet and rivulet depend on their volume V (for given contact angles, inclination and fluid properties), the droplet and rivulet volume along the height (moving distance) h can be obtained as a numerical solution for given condensation heat flux q. Once the volume is obtained, the velocity, wetting area, and average thickness can also be calculated simultaneously. According to the transition criterion (discussed later), the critical height h_t and the critical droplet volume V_t are obtained, at which the transition from moving droplet to rivulet happens.

$$V = V_0 + \Delta V_{cond} = V_0 + \int_0^h \frac{Aq}{\rho \Delta h_{fg}} \cdot \frac{dz}{u} \tag{1}$$

In order to complete the calculation of single trace, the following separate models of different flow patterns are requisite.

2.1.1. Droplet model

2.1.1.1. Onset of motion. Water droplet can rest on inclined surfaces by surface tension. The retention of water droplet is particularly significant for static droplet on the verge of sliding on inclined surfaces. The

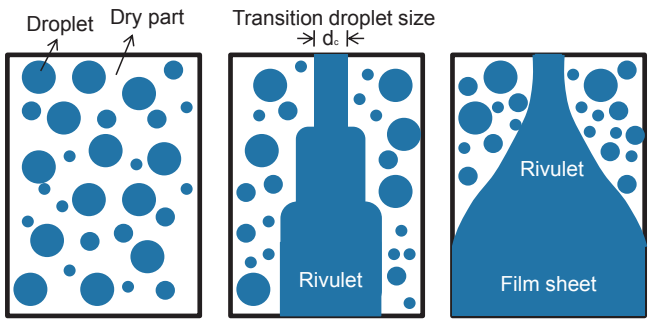

Fig. 1. Schematic of condensate flow patterns.

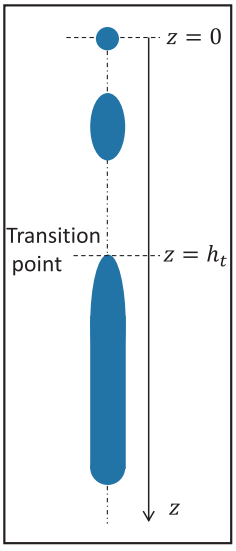

Fig. 2. Schematic of microscopic treatment.

droplet size at the onset of motion (velocity is 0) is determined with the force balance:

$$F_g = F_\sigma \tag{2}$$

The gravitation F_g and the surface tension force F_σ are:

$$F_g = V\rho g\ sin\alpha \tag{3}$$

$$F_\sigma = 2r\sigma_{LG}\ (cos\ \theta_{s,R} - cos\ \theta_{s,A}) \tag{4}$$

where r is the radius of droplet wetting area, σ_{LG} is the surface tension of the liquid–gas interface (here, water–air interface), $\theta_{s,A}$ and $\theta_{s,R}$are the apparent static advancing and receding contact angle, respectively.

These two contact angles are dependent on the physical and chemical properties of surface. For the ideal chemically homogenous and topographically smooth surface, $\theta_{s,A} = \theta_{s,R}$. But this is however not true in the case of real surfaces. On a real surface, e.g. the rough surface, the contact angle is the angle between the tangent to the liquid–vapor interface and the local solid surface, which actually exhibits a range between the advancing and receding contact angle for real surface. We see in particular that both the apparent advancing and receding contact angle and the contact angle hysteresis can be dramatically affected by the surface roughness. The relationship between roughness and wettability was defined already in refenrence (Wenzel, 1936), where it stated that adding surface roughness will enhance the wettability caused by the chemistry of the surface. For example, if the surface is chemically hydrophobic (contact angle larger than 90°), it will become even more hydrophobic when surface roughness is added.

In order to evaluate the relationship between gravitation and surface tension force, the Bond number is often adopted, which is defined as:

$$Bo = \frac{\rho V^{2/3} g sin\alpha}{\sigma_{LG}} \tag{5}$$

where ρ is the density, g is the acceleration of gravity, V is the droplet volume, α is the surface inclination angle. The critical Bond number (Bond number at the onset of motion) Bo_c is in terms of the static advancing and receding contact angle. Reliable prediction of the onset volume depends on knowing the geometry of the droplet and the forces acting on it at the onset conditions. (Dussan, 1985) derived an equation to approximate the onset volume for the case of small droplet with small contact angle hysteresis ($\theta_{s,A} - \theta_{s,R} < 10^{\circ}$). (ElSherbini and Jacobi, 2006) proposed another fomula (which used in this paper) without contact angel hysteresis limitation:

$$Bo_c = \frac{24}{\pi^3}\left(\frac{24}{\pi}\right)^{1/3} \frac{(cos\theta_{s,R} - cos\theta_{s,A})\sin\frac{\theta_{s,A}+\theta_{s,R}}{2}}{\left(2 - 3cos\frac{\theta_{s,A}+\theta_{s,R}}{2} + \cos^3\frac{\theta_{s,A}+\theta_{s,R}}{2}\right)^{1/2}} \tag{6}$$

So, for given static contact angles, we can find the critical Bond number Bo_c. Then for given inclination and fluid properties additionally, the droplet volume at its onset of motion V_0 is obtained.

2.1.1.2. Droplet geometry. Once water droplet starts moving, it is clear that the droplet shape, e.g. contact angles, depend on velocity. The shape doesn't change much with low velocity. When droplet moves fast, the dynamic advancing contact angle $\theta_{d,A}$ increases, but the dynamic receding angle $\theta_{d,R}$ decreases with the growth of droplet velocity. To simplify the real droplet geometry model, droplet shape is often approximated as a spherical cap (Meric and Erbil, 1998). The droplet radius can be given:

$$r = \left(\frac{3V}{\pi}\frac{sin^3\,\theta_e}{2 - 3cos\theta_e + cos^3\,\theta_e}\right)^{1/3} \tag{7}$$

with the equilibrium contact angle:

$$\theta_e = (\theta_{s,A} + \theta_{s,R})/2 \tag{8}$$

Then the wetting area $A = \pi r^2$ and the average thickness $\delta = \frac{V}{A}$ can be obtained.

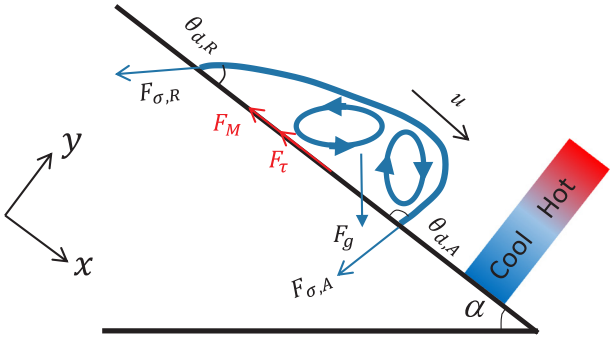

Fig. 3. Forces acting on moving droplet.

2.1.1.3. Droplet velocity. When the droplet volume (due to the condensation) becomes larger than the threshold value for the onset of motion, the droplet sliding occurs. In addition to the gravitation force and the surface tension force, the viscous force should be considered to evaluate the moving droplet velocity. Nevertheless, the Marrangoni effect on droplet velocity should be also considered, because the surface tension gradient, caused by the temperature gradient between the cool solid surface and the hot gas bulk, influences the droplet velocity as an equivalent Marrangoni force acting on the droplet. Therefore, the droplet force balance should be rewriten as:

$$F_g = F_\sigma + F_\tau + F_M \tag{9}$$

where F_τ is the viscous forces; F_M is the Marrangoni force, as shown in Fig. 3.

The viscous force F_τ is determined by the velocity gradient inside the droplet. The velocity gradient is assumed as a linear distribution: $\frac{\partial u}{\partial y} = \frac{u}{\delta}$, when the droplet moves slowly (Podgorski et al., 2001; Kim et al., 2002). In this paper, we assume droplets move fast, the velocity gradient can be approximate (Wang and Cheng, 2018):

$$\frac{\partial u}{\partial y} = \frac{u\sqrt{Re}}{r} \tag{10}$$

So the viscous force:

$$F_\tau = \pi r^2 \mu \frac{\partial u}{\partial y} = \pi r \mu u \sqrt{Re} \tag{11}$$

The droplet Reynolds number is defined as $Re = \frac{\rho u r}{\mu}$.

The equivalent Marrangoni force F_M acting on droplet, as shown in Fig. 3. The basic expression structure of the equivalent Marrangoni force comes from the references (Gallaire et al., 2014; Won et al., 2017). Namely, the Marrangoni force can be expressed empirically proportionally to the product of the change of surface tension $\Delta\sigma_{LG}$ and the droplet diameter $2r$. The proprtional constant is also related to the given droplet size. The empirical expression is valid for the case which the surface tension changes in the droplet moving direction.

However, in our case, the surface tension (as well as the temperature) changes perpendicularly to the droplet moving direction. Besides, it indicates in literature that two Marrangoni convections inside the droplet occur due to surface tension gradient in advancing and receding part respectively (Phadnis and Rykaczewski, 2017), as also shown in Fig. 3. The attractive effect (droplet moving direction) of advancing sub-convection and the repulsive effect (opposite droplet moving direction) of receding sub-convection depend on the dynamic advancing and receding contact angle, respectively. Both of these two effects have the same surface tension change $\Delta\sigma_{LG}$. With respect to the force acting distance, we couple the receding contact angle in the repulsive part as $2r{\bullet}cos\theta_{d,R}$, and the advancing contact angle in the attractive part as $2r{\bullet}cos\theta_{d,A}$. Therefore, when we combine both the repulsive and the attractive part, one obtains the proposed Marrangoni force expression as

follows:

$$F_M = \Delta\sigma_{LG} \cdot [2r(cos\theta_{d,R} - cos\theta_{d,A})] \tag{12}$$

with

$$\Delta\sigma_{LG} = \frac{\partial\sigma_{LG}}{\partial T}\frac{\partial T}{\partial y}\Delta y \tag{13}$$

where $\frac{\partial\sigma_{LG}}{\partial T}$ is the surface tension gradient with respect to temperature; $\frac{\partial T}{\partial y}$ is temperature gradient in y- direction; Δy is droplet height in y-direction (approximates the droplet thickness δ). The droplet velocity depending on droplet size can be then derived from the updated force balance Eq. (9):

$$\rho V g sin\alpha = 2r(\sigma_{LG} + \Delta\sigma_{LG})(cos\theta_{d,R} - cos\theta_{d,A}) + \pi r\mu u\sqrt{Re} \tag{14}$$

We can see the Marrangoni force can combine with surface tension force, which seems the Marrangoni effect modifies the surface tension consequently.

If the droplet geometry is not so sensitive to droplet velocity that the dynamic advancing and receding contact angle can be replaced by static advancing and receding contact angle. However, in this study the water droplet has a relative high velocity, the following empirical correlation of dynamic contact angles is adopted (Wang and Cheng, 2018):

$$(cos\theta_{d,R} - cos\theta_{d,A}) = 0.32We^{0.303}(1 - cos\theta_{s,e})^{-0.747} + (cos\theta_{s,R} - cos\theta_{s,A}) \tag{15}$$

where the droplet Weber number is $We = \frac{\rho u^2 r}{\sigma_{LG}}$.

2.1.2. Transition criterion

The transition from moving droplet to rivulet is a very complicated process. The surface tension, which makes the droplet acquire the least surface area, shapes the droplet structure. We artificially separate a droplet into two parts. It is reasonable to assume that there is a pair of action $F_{i,21}$ and reaction $F_{i,12}$ forces acting on the interface between these two parts, as shown in Fig. 4. The interface action force can be calculated by, e.g. for part 1,

$$F_{i,21} = F_{g,1}sin\alpha - F_{\tau,1} - F_{\sigma,1} - F_{M,1} \tag{16}$$

$$F_{i,21} = \rho V_1 g sin\alpha - A_1\mu\frac{\partial u}{\partial y} + 2r_1(\sigma_{LG} + \Delta\sigma_{LG})cos\theta_{d,A} \tag{17}$$

where the subscript 1 is for droplet part 1.

When the surface tension force at the interface is less than the required action force on the interface, namely, $F_{\sigma,21} < F_{i,21}$, the structure will be stretched, which means the transition from droplet to rivulet starts. The surface tension force is:

$$F_{\sigma,21} = \sigma_{LG} \cdot d_h \tag{18}$$

d_h is the hydraulic diameter of the interface:

$$d_h = 2r\frac{\left(\frac{\theta_e}{sin\theta_e} - cos\theta_e\right)}{\theta_e + sin\theta_e} \tag{19}$$

In this paper, the transition droplet size is obtained by solving the criterion by iteration. For understanding of the transition process, if the viscous force is neglected (namely, if surface tension force much larger than viscous force, $F_{\sigma,1} \gg F_{\tau,1}$), then the transition criterion can be simplified (roughly separate the droplet into two equal parts) as:

$$\rho\frac{V_t}{2}gsin\alpha - r_t(\sigma_{LG} + \Delta\sigma_{LG})cos\theta_e = 2r_t\sigma_{LG}\frac{\left(\frac{\theta_e}{sin\theta_e} - cos\theta_e\right)}{\theta_e + sin\theta_e} \tag{20}$$

$$Bo_t = \frac{\rho V_t^{2/3} g sin\alpha}{\sigma_{LG}} = \frac{2\left(2\frac{\left(\frac{\theta_e}{sin\theta_e} - cos\theta_e\right)}{\theta_e + sin\theta_e} + cos\theta_e\left(1 + \frac{\Delta\sigma_{LG}}{\sigma_{LG}}\right)\right)}{\left(\frac{\pi(2 - 3cos\theta_e + cos^3\theta_e)}{3sin^3\theta_e}\right)^{1/3}} \tag{21}$$

Actually the Bond number at the transition, Bo_t, might be under estimated due to the neglect of the droplet viscous force. The transition size V_t or r_t can be obtained easily by the Bo_t. It is clear that the transition point is dependent on the contact angle, inclination and fluid properties. There is no fixed, constant value for any kind of surfaces.

2.1.3. Rivulet model

The initial rivulet structure after the droplet transition is the first issue solved in the rivulet model. The minimum total energy (MTE) method is applied for determining the rivulet thickness of an isothermal rivulet flowing down a sloped wall. In previous researches (Doniec, 1988; El-Genk and Saber, 2001; Huang and Cheng, 2015), analytical expressions of a stable rivulet, such as two dimensional geometry and velocity profile, are developed. One of the empirical rivulet thickness δ results is:

$$\delta = 1.45(1 - cos\theta_e)^{0.2}[\mu^2\sigma_{LG}/(\rho^3(gsin\alpha)^2)]^{0.2} \tag{22}$$

The initial rivulet half width (one arc part, as seen in Fig. 5)

$$a = \frac{sin\theta_e}{1 - cos\theta_e}\delta \tag{23}$$

The initial rivulet geometry profile (the thickness in the two side arc parts)

$$\phi(x) = \delta - \frac{\delta}{1 - cos\theta_e}\left[1 - \sqrt{1 - x^2\left(\frac{1 - cos\theta_e}{\delta}\right)^2}\right], -a \le x \le a \tag{24}$$

and the rivulet velocity profile:

$$u = \frac{\rho g sin\alpha}{\mu}\left(y\phi - \frac{\phi^2}{2}\right) \tag{25}$$

The previous researches suggest that the spread of rivulet width happens while the condensate increases continuously, but the rivulet thickness keeps at the initial value, as shown in Fig. 5. When the volume flow rate increases, the rivulet spreads at both sides, and a rectangular film sheet forms in the middle.

2.2. Macroscopic treatment

Based on the above microscopic treatment, the second step of the modeling approach is the integral of all the isolated single traces of droplet and rivulet. We call it macroscopic treatment, whoes schamictic as shown in Fig. 6. In order to figure out the amount of droplets and

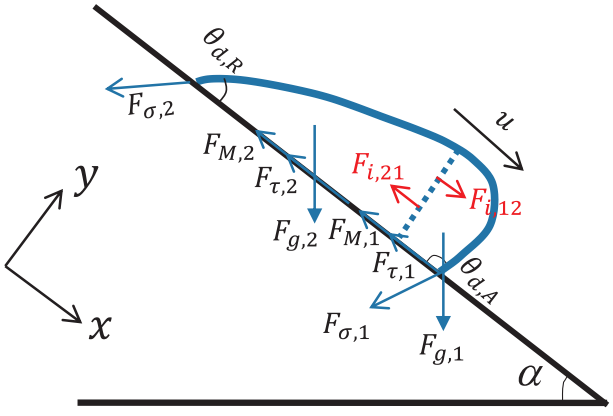

Fig. 4. Forces acting on moving droplet at transition.

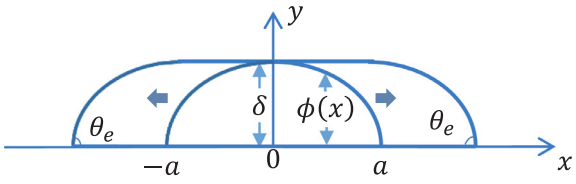

Fig. 5. Rivulet structure.

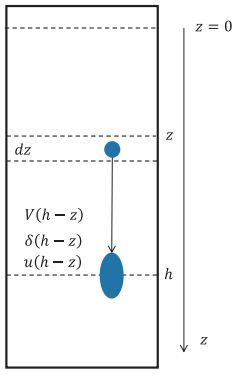

Fig. 6. Schematic of macroscopic treatment.

rivulets generated on the surface, the droplets initiation density n (unit: $1/(m^2{\cdot}s)$, droplets generation number per area and per time) is introduced. The droplets initiation density can be expressed as:

$$n = \frac{q}{\Delta h_{fg}\bullet\rho\bullet V_0}(1-\varepsilon) \tag{26}$$

where Δh_{fg} is the specific latent heat of vapor condensation and ε is the coverage rate. $(1-\varepsilon)$ means the non-covered area fraction, which means the initiation of moving droplet only occurs in the non-covered area (i.e. non-wetting area). The new initiated moving droplet rate per width (unit: $1/(m{\cdot}s)$) in the interval dz at each elevation h (as shown in Fig. 6) is:

$$n\bullet dz = \frac{q}{\Delta h_{fg}\bullet\rho\bullet V_0}(1-\varepsilon)\bullet dz \tag{27}$$

The volume flow rate per width $\dot{V}$, $m^3/(m{\cdot}s)$, at each height h is the integration from the top of structure $z=0$ to the height h, which can be calculated by:

$$\dot{V} = \int_0^h V(h-z)ndz \tag{28}$$

It is notable that the volume of condensate (droplet and rivulet) using in the integral equation should consider the moving distance from the droplet initial position to the position of interest. So the volume in Eq. (28) is $V(h-z)$ rather than $V(z)$, as shown in Fig. 6. The volume for each specific droplet and rivulet can be obtained in the microscopic treatment as well as the thickness $\delta(h-z)$ and velocity $u(h-z)$. The average thickness $\bar{\delta}$ and velocity $\bar{u}$ can be also obtained as below:

$$\bar{\delta} = \frac{\int_0^h \delta(h-z)ndz}{\int_0^h ndz} \tag{29}$$

$$\bar{u} = \frac{\int_0^h \rho V(h-z)\bullet u(h-z)ndz}{\int_0^h \rho V(h-z)ndz} \tag{30}$$

where the average thickness is weighted by the total amount of droplets and rivulet, and the average velocity is weighted by the total mass of them.

Afterwards, the coverage rate averaged over plate surface can be obtained by:

Table 1
Experimental data for validation.

Experiment	Re	$\theta_{s,A}/\theta_{s,R}$	Inclination	Temperature	Data points
WEBREC	10 500	71. 8°/18. 4°	90°	Ambient	21
	20 110	18°/10°	90°	Ambient	15
Ausner, 2007	30 240	65°/	60°	Ambient	43
THAI-AW3-LAB	261 285	θ_e=60 65°	2°, 10°, 20°	Ambient	6
LINX	18 62	65°/45°	90°	67 113 °C	4

$$\varepsilon = \frac{\dot{V}}{\bar{u}\bullet\bar{\delta}} \tag{31}$$

Actually the variable height h plays a role as an intermediate variable. All output parameters (such as coverage rate, average thickness and velocity) is a one-to-one relationship with the condensate volume flow rate. It is clear that the current modeling approach can present the output parameters in dependence on condensate volume flow rate $\dot{V}$, so that the modeling approach is feasiable to be applied to containment lamped parameter codes.

3. Validation

Four experiments including 89 experimental data points from the open literature are applied to validate the current condensate coverage rate model (Yu et al., 2012; Ausner, 2007; Laufenberg et al., 2014; Dupont, 2017). The information of these experimental data for validation is summarized in Table 1. Most of the data are often expressed as Reynolds number which is defined as $Re = \frac{4\rho\dot{V}}{\mu}$. Actually not all contact angles are given by each individual experiment, but the surface materials are exactly given. Most of the experiments are without condensation effect and conducted under the ambient temperature and pressure, while the LINX experiment is under the real containment condensation condition.

However, the condensation effect in our model, actually, is equivalent to the condensate volume flow rate increase or decrease. Even in some condensation experiments, especially on the non-cooling walls, rivulets (only rivulets, without droplets) are often observed due to the condensate falling from the upper cooling walls, e.g. in experiments THAI-AW3 and LINX. This phenomenon may also happen in the containment during accidents.

It is remarkable that, in WEBREC, Ausner's and THAI-AW3-LAB experiments, rivulets form directly by water injection on the top of the test structures. The coverage rate depends on the injection water volume flow rate.

So these three experiments are adopted to validate the rivulet coverage rate. The validation work is carried out one by one in the following sections.

3.1. WEBREC experiment

The facility WABREC (WAter Behavior in REctangle Channel) consists of a vertical stainless plate which is 2 m wide and 5 m long. The surface of the plate is painted with organic/inorganic zinc coating. Rivulet forms on the vertical plate when the water overflows reserve tank. Water temperature is kept constant at 25 °C while the pressure is ambient. More information about WABREC experiment, please refer to (Yu et al., 2012).

WABREC rivulet experiment (without droplets) considers two paints, but only the contact angles of inorganic zinc coating are known for us. So we take the tests on inorganic zinc coating to compare with our model prediction. Two sets of coverage rate are measured at two different surface conditions (wet plate and dry plate) with the change of the volume flow rate.

Since there are only rivulets in WEBREC experiment, we make all droplets transfer to rivulets immediately after droplets generate on surface. In the modeling approach, let $V_t = V_0$, which means all condensate exist in form of rivulets.

Fig. 7 shows the comparison between the model prediction and the WEBREC experimental data. The comparison results indicate a good agreement. The predicted relationship between the coverage rate and Reynolds number is almost linear (parabolic actually), because the average rivulet thickness and velocity don't increase much when volume flow rate increases. We look at the coverage rate formula $\varepsilon = \frac{\dot{V}}{\bar{u} \cdot \delta} = \frac{\mu}{4\rho\bar{u} \cdot \delta} \cdot Re$. It is clear that the slope of the curve is more or less $\frac{\mu}{4\rho\bar{u} \cdot \delta}$ if the rivulet average thickness and velocity are fixed.

Another issue of interest is about the effect of contact angle. The test condition difference between wet and dry test surface is the contact angle, but the coverage rate results are quite different at the same Reynolds number. The lower equilibrium contact angle (wet surface) is, the faster the coverage rate increases with the Reynolds number, because the equilibrium contact angle effects the rivulet thickness and velocity much (see the rivulet model section). Smaller equilibrium contact angle leads to smaller rivulet thickness and lower rivulet velocity.

3.2. Ausner's experiment

The rivulet flow behavior is observed with a CCD camera in Ausner's experiment (Ausner, 2007). The pictures are used to obtain the information on the wetted surface area. To obtain different inlet conditions the liquid can either be fed onto the plate out of a tank with an overflowing weir or through a feeding tube with several holes. Experiment investigates the rivulet coverage (without droplets) over Reynolds number for water on a 60° inclined steel plate.

The steel plate used in the experiments is not treated before the measurements. The plate is a rough surface. The static contact angle (it is mentioned like that in (Ausner, 2007)) measured varies between 60° and 70° with a measurement error 6–9°. Here we think it is the static advancing contact angle since it is measured on a dry steal surface. The simulation here uses an average advancing contact angle of 65°. The receding contact angle is hypothetically taken as 12° to make the contact angle hysteresis as the same as other steal surface. Moreover, because there are only rivulets in Ausner's experiment, we make all droplets transfer to rivulets immediately after droplets generate as well as in the calculation of WEBREC case.

In Fig. 8, it can be seen that the simulated coverage rate agrees well with the experimental data. Anyway the rivulets cover less area in prediction than in the experiment when the plate approaches to fully cover. Furthermore, the experimental data themselves also have a large deviation at a specific identical *Re*. This characteristic can be explained as the effect of the contact angle. The steel plate used is a non-treated surface, the surface is so heterogeneous that the contact angle would change in a large range.

3.3. THAI-AW3-LAB experiment

THAI-AW3-LAB Experiment is one of the experiments series of aerosol wash down experiments conducted by Becker Technologies (Laufenberg et al., 2014; Gupta, 2015; Amend et al., 2018; Freitag et al., 2018). THAI-AW3-LAB is a laboratory scale experiment to investigate the aerosol wash down behavior. Some of tests (such as test 3, test 4 and test 12) can be used to validate the rivulet behavior and coverage rate. The experimental setup consists of trapezoidal inclined plates loaded with insoluble silver aerosol. The plates are made out of steel and have two surfaces types (stainless steel and decontamination paint). At the uppermost edge purified water is applied on the plate by a water distributor with a given mass flow rate. A tubular distributor (with 38 holes of 0.7 mm diameter along the edge) is used to generate a homogeneous water distribution. Pictures of the water flow are recorded during the tests. These images are used to identify the wetting area of the plates as well as the flow pattern of rivulets. For further information, THAI-AW3-LAB laboratory experiments report (Laufenberg et al., 2014) is recommended.

The inclinations of test 3, 12 and 4 are 2°, 10° and 20° respectively. These tests are conducted under ambient pressure and temperature. The mass flow rate is the same, 11 g/s. The trapezoidal plate upper width is 0.475 m, and the lower width is 0.09 m, so the average $Re = \frac{4\rho\dot{V}}{\mu} = 175$. The surface of test 3 and 4 are stainless steel coating with GEHOPON paint, while the test 12 without any paint. The water on GEHOPON paint has an equilibrium static contact angle 60–65°, here we take the average 62.5°. We make all droplets transfer to rivulets immediately after droplets generate as well as in WEBREC and Ausner's cases (only rivulet, no droplet).

Table 2 reveals the comparison of the rivulet average thickness and velocity. The average value at 900 sec of each THAI-AW3-LAB test are selected (We only have this moment data from von Laufenberg et al., 2014). Both the experiment and calculation results show that the rivulet average thickness decrease with the inclination increasing, on the contrary, the rivulet average velocity increase. The results are consistent with the rivulet thickness and velocity model, which are both in terms of inclination angle, roughly $\bar{\delta} \propto sin\alpha^{-0.4}$ and $\bar{u} \propto sin\alpha^{0.2}$ if *Re*, contact angle and water propoties keep constant.

Fig. 9 shows the coverage rate comparison between calculations and THAI-AW3-LAB tests. The coverage rate increases a little with inclination angle increasing. However, it seems that the inclination effect is not significant beyond a certain value. The result is also consistent with the rivulet coverage rate model prediction, roughly $\varepsilon \propto sin\alpha^{0.2}$, when *Re*, contact angle and water propoties keep constant.

3.4. LINX experiment

The LINX condensation experiments are conducted by PSI in Switzerland. The LINX facility consists of a single stainless steel vessel with 2 m diameter and 3.4 m high (10 m^3 in volume). A vertical cooling wall, 0.4 m wide and 2.1 m high, consisting of 9 aluminum blocks was built in the center of the pressure vessel (Dupont, 2017). The blocks are covered by a single 0.7 mm thick aluminum sheet. The mass flow rate of cooling water is independently controlled and its inlet and outlet temperature are measured for each block, in order to calculate the average heat removal from containment.

The surface of the metal sheet has undergone a chemical etching

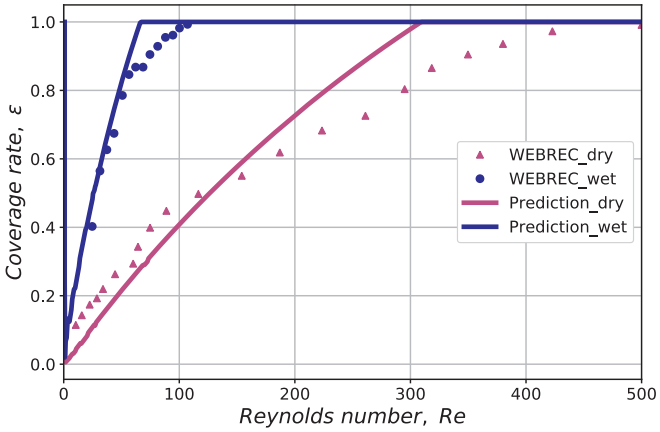

Fig. 7. Comparison with WEBREC experimental data. The boundary conditions of the calculation are exactly the experiment conditions: the static contact angles $\theta_{s,A}/\theta_{s,R}$ are 71. 8°/18. 4° for dry surface and 18°/10° for wet surface; the inclination angle $\alpha = 90°$ for a vertical wall; the temperature and pressure are ambient; last it doesn't matter how much the condensation heat flux is (see the chapter 4).

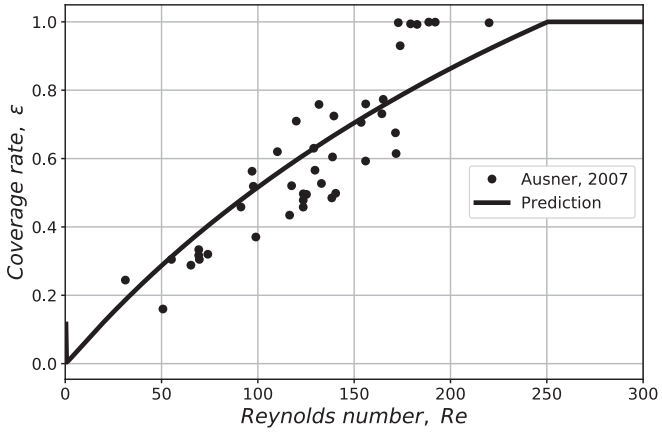

Fig. 8. Coverage rate plotted over the Reynolds number for the case of Ausner's experiment. Boundary conditions: the static contact angles $\theta_{s,A}/\theta_{s,R}$ are 65°/12°; the inclination angle $\alpha = 60^{\circ}$ of inclined steel plate; the temperature and pressure are ambient.

Table 2
Rivulet parameters comparison (average at 900 sec of THAI-AW3-LAB).

	$\bar{\delta}$, mm	$\bar{u}$, m/s
Test3/Calculation	0.62/1.0	0.137/0.1
Test12/Calculation	0.41/0.55	0.23/0.16
Test4/Calculation	0.31/0.42	0.27/0.20

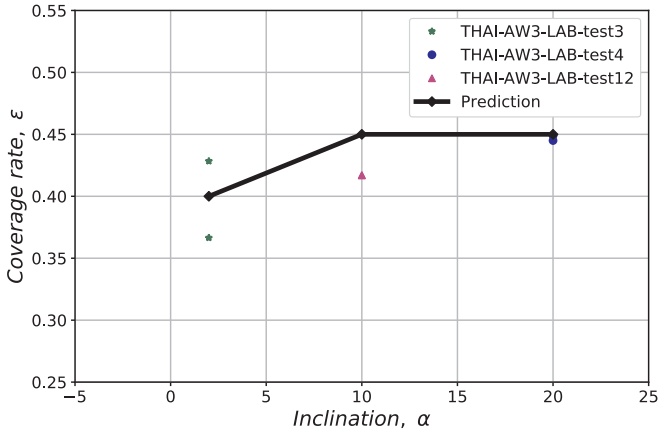

Fig. 9. Coverage rate vs plate inclination comparing with THAI-AW3-LAB.

treatment. The static advancing and receding contact of water on the plate are 65° and 45° respectively. The average temperature is 95 °C and the pressure is 1.1 bar. 4 tests (test 210, 215, 211, 216) of rivulets are conducted under condensation condition and without water injection at the uppermost plate (Dupont, 2017). The condensation mass flow rate per width at the picture captured area are 2.7 g/(s·m), 2.9 g/(s·m), 4.3 g/(s·m), 5.2 g/(s·m) respectively calculated by energy balance, and the Reynolds number are 35.5, 38.6, 57, 70 respectively.

Fig. 10 shows the calculation results of rivulet coverage rate for the given boundary condition of LINX. Compared with LINX experiment, the prediction of test 210 and 215 is much closer to the experimental data, while there is a large deviation of test 211 and 216. Because test 211 and 216 contain many droplets covered on the surface (see the bottom-right subfigures in Fig. 10). Unfortunately, we can't distinguish the moving droplets and the static ones in test 211 and 216. Otherwise we can compare the whole moving liquid wetting area with the present model directly.

4. Results and discussions

In this chapter the developed model is applied to simulate the condensate flow behavior under prototypical conditions: the static advancing and receding contact angles are 71.8° and 18.4° respectively since these two angles are the experiment measured values for water on a dry containment paint (Inorganic zinc coating) coated stainless steel (Wang and Cheng, 2018). The inclination angle $\alpha = 90^{\circ}$ for a vertical wall. The condensation heat flux is given as 50 kW/m^2 (actually the condensation heat flux range in containment is about 1–100 kW/m^2 during accident, in reference (de la Rosa et al., 2009)). The pressure of atmosphere and temperature of water are assumed 4 bar and 90 °C, respectively to obtained the fluid properties. The temperature difference between bulk and solid cooling wall is in range 10–60 (Herranz et al., 2007). Here we take the average temperature difference 35 °C to calculate the equivalent Marrangoni effect on surface tension.

For these above given contact angles, inclination angle, condensation heat flux and fluid properties, the numerical solution of the droplet and rivulet volume, velocity, wetting area, average thickness along the wall height are shown in Fig. 11.

The condensate (droplet and rivulet) volume increases monotonously with the moving distance, as shown in Fig. 11. It is continuous no matter before or after the transition occurs ($h_t = 1.2$ in the current case). But the slope of this curve changes between the droplet and rivulet flow pattern due to its wetting area and velocity alter, as shown in Eq. (1).

During the droplet phase, the velocity, wetting area and thickness increase with droplet volume, as well as these quantities in rivulet phase. However, the velocity, wetting area and thickness have a step change before and after the transition, because of the difference of geometry and velocity between droplets and rivulets. The droplet wetting area and velocity are much smaller than those of rivulet, but the thickness on the contrary. In addition, the velocity and thickness of rivulet at beginning increase slightly, and at the end both of them are stable. Since the rivulet width spreads with the condensate volume continuously, and a rectangular film sheet forms in the middle with a fixed thickness calculated by MTE method. That means the proportion of the two arc parts of rivulet becomes less important when the rectangular film sheet becomes wider.

Based on the above microscopic treatment's results, and according to our macroscopic treatment, volume flow rate per width and average thickness, velocity and coverage rate are obtained as a function of height respectively, as shown in Fig. 12. The volume flow rate per width

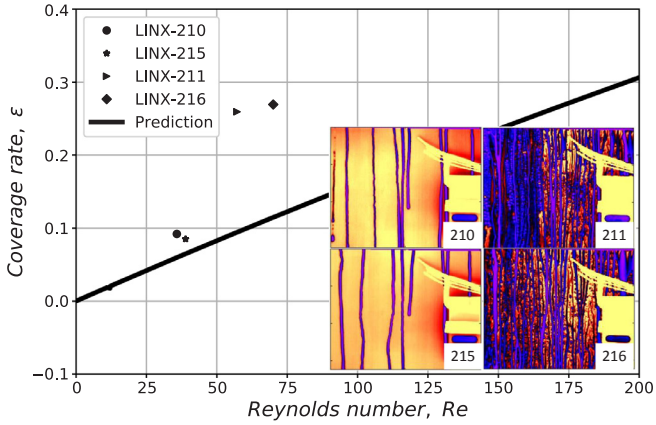

Fig. 10. Rivulets coverage rate comparison between prediction and LIXN tests. The four subfigures in bottom-right are the picture of test 210, 215, 211, 216 from (Dupont, 2017). Color blue means water covered area. The area ratio is obtained by the software ImageJ process. (For interpretation of the references to color in this figure legend, the reader is referred to the web version of this article.)

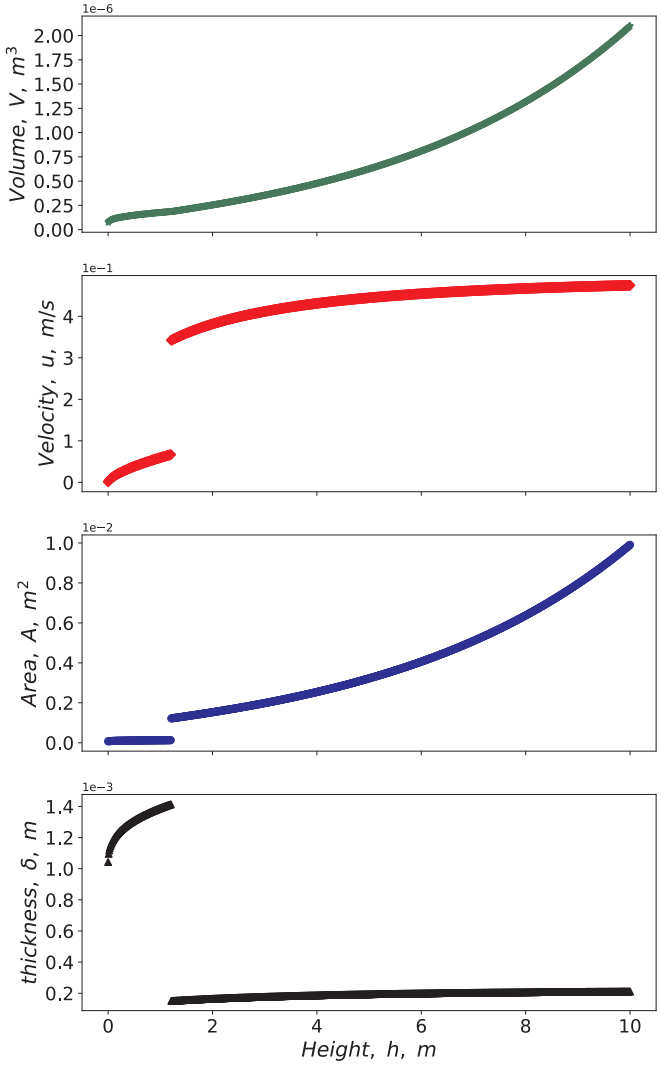

Fig. 11. Microscopic treatment results for one single trace.

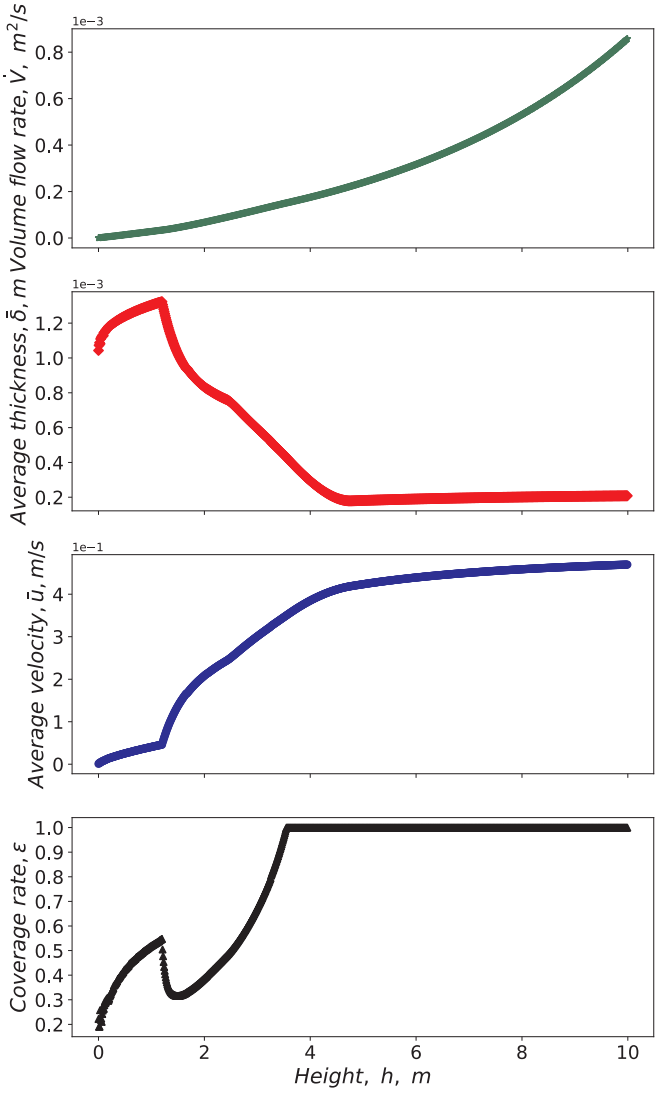

Fig. 12. Macroscopic treatment results for the integral effect.

increases over the moving distance. Because the total number (integral along height) of droplets and rivulets increase, as long as the initiation density $n \geq 0$ (which is true according to Eq. (26).

The average thickness and velocity change much when the transition happens, since the thickness, velocity models vary dramatically after transition. Before transition, all the condensate are droplets, after the transition the condensate consists of droplets and rivulets. Therefore, during the coexisting phase, the average thickness decrease but the velocity increase obviously, since the rivulet is a very thin liquid layer and flow downwards faster. Later, most droplet grows and transfers to rivulet, then the rivulet dominate the condensate flow. That is why the average thickness and velocity are stable at 0.22 mm and 0.486 m/s respectively (both values can also be obtained by rivulet model Eqs. (22) and (25) independently).

For using the numerical results in COCOSYS code, probably the volume flow rate, contact angles, inclination and fluid properties are known as inputs for coverage rate calculation. From the macroscopic results in Fig. 12, both the volume flow rate and the coverage rate are one-to-one relationship with height h. When the intermediate variable h is eliminated, the function between coverage rate (dependent variable) and volume flow rate (independent variable) is obtained as shown in Fig. 13 (The blue dot is the results of the current case). In the same way, the average thickness and velocity, as well as the flowing condensate coverage rate, are also in terms of volume flow rate, contact angles, inclination and fluid properties, and can be obtained by the current modeling approach.

The coverage rate alters much when the transition occurs, as shown in Fig. 13. Coverage rate rises moderately during the droplet phase, then declines rapidly since the product of average thickness and velocity increase much after transition. Later the coverage rate recovers and

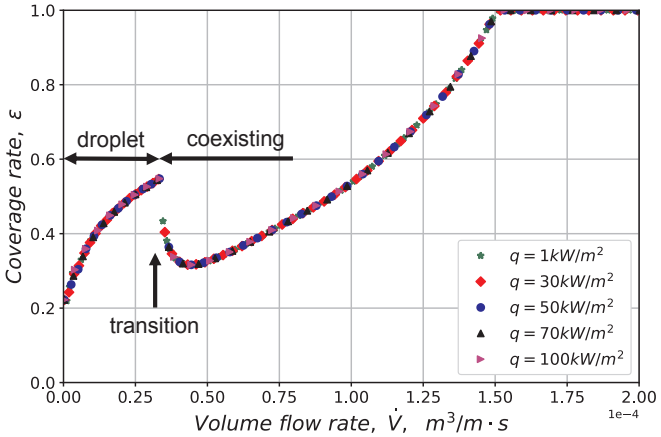

Fig. 13. Coverage rate vs volume flow rate with different condensation heat flux.

climbs during the coexisting phase, because the product of average thickness and velocity drops.

From the transition criterion, the size of droplet V_t and r_t are known for given contact angles, inclination and fluid properties. Moreover based on the microscopic treatment, the critical height h_t are known by Eq. (1). Therefore, the critical volume flow rate:

$$\dot{V}_t = \int_0^{h_t} V(h-z)ndz \tag{32}$$

In current case the $\dot{V}_t$ is $0.336{\cdot}10^{-4}\,m^3/(m{\cdot}s)$.

Fig. 13 also shows the coverage rate plotted over volume flow rate with different condensation heat flux. It is obvious that the coverage rate, as well as the volume flow rate, will increase at a certain height while the condensation heat flux increase. However, it doesn't matter to change the condensation heat flux when we focus on the relationship between the coverage rate and volume flow rate. The volume flow rate is the integral of the condensation heat flux along height, as expressed in Eq. (26). In other words, the volume flow rate represents already the effect of condensation heat flux.

5. Conclusions

The flowing condensate coverage on inclined wall is a significant factor for evaluating the aerosol wash down efficiency. A modeling approach of the flowing condensate coverage rate is proposed, which contains a microscopic treatment and a macroscopic treatment. The coverage rate is a function of volume flow rate, contact angles, inclination and fluid properties.

Droplet and rivulet model from literatures used in the current modeling approach are presented. We propose an equivalent Marrangoni force expression to consider its effect on droplet velocity. Moreover, these is no existing transition criterion in the open literature to describe the transition from droplet to rivulet. So a transition criterion is proposed in this paper based on the assumption that when the surface tension force is less than the action force on the interface inside a droplet, the droplet structure will stretch to rivulet.

The modeling approach is validated by the existing experimental data. Generally speaking, the comparisons indicate that, the predictions of rivulet coverage rate by the current modeling approach agree well with the experimental data.

Effects of *Re* number, contact angle and inclination angle on rivulet coverage rate are obtained. The rivulet coverage rate increases almost linearly with Re number, increases rapidly as the equilibrium static contact angle decreases, increases with inclination angle when it is small and keeps nearly unchanged when it is large.

The new model is applied to a basic and prototypical case (a normal case for nuclear containment accident). Numerical results seem the droplet phase cannot be neglected under a real condensation condition, especially on a dry surface with a large equilibrium contact angle. The calculations show the volume flow rate represents already the effect of condensation heat flux on coverage rate.

In the future, in order to implementing the present model in the containment program COCOSYS for the aerosol wash down calculation, empirical correlations will be developed to predict the coverage rate, average velocity in dependence on volume flow rate, contact angle, inclination and thermophysical properties based on the proposed model.

Acknowledgments

This work is supported by the project "Erweiterung des Strömungsmodells zur Simulation des Aerosolabwaschens (ESSA, grant number: 1501537)", funded by the German Federal Ministry of Economic Affairs and Energy(BMWi). We thank our partners and colleges from Becker Technologies and GRS for experimental data support and many fruitful discussions.

Reference

Amend, K., Klein, M., München, U.D.B., Weg, W.H., 2018. Modeling and Simulation of water flow on containment walls with inhomogeneous contact angle distribution. ATW Int. J. Nucl. Power 62 (7), 477 481.

Ausner, I., 2007. Experimentelle Untersuchungen mehrphasiger Filmströmungen. PhD Thesis.

de la Rosa, J.C., Escrivá, A., Herranz, L.E., Cicero, T., Muñoz-Cobo, J.L., 2009. Review on condensation on the containment structures. Prog. Nucl. Energy. https://doi.org/10.1016/j.pnucene.2008.01.003.

Doniec, A., 1988. Flow of a laminar liquid film down a vertical surface. Chem. Eng. Sci. 43 (4), 847 854.

Dupont, J., 2017. Thin liquid film dynamics in a condensing and re-evaporating environment. Phys. World. https://doi.org/10.1088/2058-7058/7/6/30.

Dussan, E.B.V., 1985. On the ability of drops or bubbles to stick to non-horizontal surfaces of solids. Part 2. Small drops or bubbles having contact angles of arbitrary size. J. Fluid Mech. 151, 1 20. https://doi.org/10.1017/S0022112085000842.

El-Genk, M.S., Saber, H.H., 2001. Minimum thickness of a flowing down liquid film on a vertical surface. Int. J. Heat Mass Transf. 44, 2809 2825. https://doi.org/10.1016/S0017-9310(00)00326-4.

ElSherbini, A.I., Jacobi, A.M., 2006. Retention forces and contact angles for critical liquid drops on non-horizontal surfaces. J. Colloid Interface Sci. 299, 841 849. https://doi.org/10.1016/j.jcis.2006.02.018.

Freitag, M., Gupta, S., Beck, S., Sonnenkalb, M., 2018. Experimental and analytical investigations of aerosol processes wash-out and wash-down. Nucl. Sci. Eng. 193, 198 210. https://doi.org/10.1080/00295639.2018.1479091.

Gallaire, F., Meliga, P., Laure, P., Baroud, C.N., 2014. Marangoni induced force on a drop in a Hele Shaw cell. Phys. Fluids 26. https://doi.org/10.1063/1.4878095.

Guo, J., 2002. Hunter rouse and shields diagram. Adv. Hydraul. Water Eng. 2, 1096 1098. https://doi.org/10.1142/9789812776969_0200.

Gupta, S., 2015. THAI experiments on volatility, distribution and transport behaviour of iodine and fission products in the containment. Proceedings of the International OECD-NEA/NUGENIA-SARNET Workshop on the Progress in Iodine Behaviour for NPP Accident Analysis and Management.

Herranz, L.E., Vela-García, M., Fontanet, J., del Prá, C.L., 2007. Experimental interpretation and code validation based on the PHEBUS-FP programme: Lessons learnt from the analysis of the containment scenario of FPT1 and FPT2 tests. Nucl. Eng. Des. 237, 2210 2218. https://doi.org/10.1016/j.nucengdes.2007.03.022.

Huang, X., Cheng, X., 2015. Modification and application of water film model in COCOSYS for PWR's passive containment cooling. Nucl. Eng. Des. 280, 251 261. https://doi.org/10.1016/j.nucengdes.2014.08.026.

Kim, H.Y., Lee, H.J., Kang, B.H., 2002. Sliding of liquid drops down an inclined solid surface. J. Colloid Interface Sci. 247, 372 380. https://doi.org/10.1006/jcis.2001.8156.

Klein-Heßling, W., Arndt, S., Weber, G., Nowack, H., Spengler, C., Schwarz, S., Pelzer, M., Eckel, J., 2015. COCOSYS v2.4 User's Manual. GRS.

Laufenberg, B. Von, Colombet, M., Freitag, M., 2014. Wash-down Tests of Silver Aerosol from Stainless Steel and Painted Surfaces. pp. 1 12.

Meric, R.A., Erbil, H.Y., 1998. Evaporation of sessile drops on solid surfaces: pseudo-spherical cap geometry. Langmuir 14, 1915 1920. https://doi.org/10.1021/la970147c.

Phadnis, A., Rykaczewski, K., 2017. The effect of Marangoni convection on heat transfer during dropwise condensation on hydrophobic and omniphobic surfaces. Int. J. Heat Mass Transf. 115, 148 158. https://doi.org/10.1016/j.ijheatmasstransfer.2017.08.026.

Podgorski, T., Flesselles, J.M., Limat, L., Kim, H.Y., Lee, H.J., Kang, B.H., 2001. Sliding of liquid drops down an inclined solid surface. J. Colloid Interface Sci. 247, 372 380. https://doi.org/10.1103/PhysRevLett. 87.036102.

Wang, F., Cheng, X., 2018. Model assessment of condensate droplet motion on inclined containment structure surface. NUTHOS-12 1 13.

Weber, G., Funke, F., Gupta, S., 2015. Iodine and Silver Wash-Down Modelling in Cocosys-Aim By Use of Thai Results. OECDNEA/NUGENIA-SARNET Work.

Wenzel, R.N., 1936. Resistance of solid surfaces to wetting by Water. Ind. Eng. Chem. 28, 988 994.

Won, B.J., Lee, W., Song, S., 2017. Estimation of the thermocapillary force and its applications to precise droplet control on a microfluidic chip. Sci. Rep. 7 (1), 3062.

Yu, Y.Q., Wei, S.J., Yang, Y.H., Cheng, X., 2012. Experimental study of water film falling and spreading on a large vertical plate. Prog. Nucl. Energy 54, 22 28. https://doi.org/10.1016/j.pnucene.2011.09.007.